



---

**Quantum Devices Based on Transition Metal Dichalcogenides**

**Hugh Churchill  
UNIVERSITY OF ARKANSAS**

---

**09/12/2019  
Final Report**

**DISTRIBUTION A: Distribution approved for public release.**

**Air Force Research Laboratory  
AF Office Of Scientific Research (AFOSR)/ RTB1  
Arlington, Virginia 22203  
Air Force Materiel Command**

DISTRIBUTION A: Distribution approved for public release.

<b>REPORT DOCUMENTATION PAGE</b>			<i>Form Approved</i> <i>OMB No. 0704-0188</i>		
<p>The public reporting burden for this collection of information is estimated to average 1 hour per response, including the time for reviewing instructions, searching existing data sources, gathering and maintaining the data needed, and completing and reviewing the collection of information. Send comments regarding this burden estimate or any other aspect of this collection of information, including suggestions for reducing the burden, to Department of Defense, Executive Services, Directorate (0704-0188). Respondents should be aware that notwithstanding any other provision of law, no person shall be subject to any penalty for failing to comply with a collection of information if it does not display a currently valid OMB control number.</p> <p><b>PLEASE DO NOT RETURN YOUR FORM TO THE ABOVE ORGANIZATION.</b></p>					
<b>1. REPORT DATE (DD-MM-YYYY)</b> 11-07-2020		<b>2. REPORT TYPE</b> Final Performance		<b>3. DATES COVERED (From - To)</b> 15 Jun 2018 to 14 Jun 2019	
<b>4. TITLE AND SUBTITLE</b> Quantum Devices Based on Transition Metal Dichalcogenides			<b>5a. CONTRACT NUMBER</b>		
			<b>5b. GRANT NUMBER</b> FA9550-16-1-0203		
			<b>5c. PROGRAM ELEMENT NUMBER</b> 61102F		
<b>6. AUTHOR(S)</b> Hugh Churchill			<b>5d. PROJECT NUMBER</b>		
			<b>5e. TASK NUMBER</b>		
			<b>5f. WORK UNIT NUMBER</b>		
<b>7. PERFORMING ORGANIZATION NAME(S) AND ADDRESS(ES)</b> UNIVERSITY OF ARKANSAS 120 N. OZARK AVENUE FAYETTEVILLE, AR 72701-1036 US			<b>8. PERFORMING ORGANIZATION REPORT NUMBER</b>		
<b>9. SPONSORING/MONITORING AGENCY NAME(S) AND ADDRESS(ES)</b> AF Office of Scientific Research 875 N. Randolph St. Room 3112 Arlington, VA 22203			<b>10. SPONSOR/MONITOR'S ACRONYM(S)</b> AFRL/AFOSR RTB1		
			<b>11. SPONSOR/MONITOR'S REPORT NUMBER(S)</b> AFRL-AFOSR-VA-TR-2020-0096		
<b>12. DISTRIBUTION/AVAILABILITY STATEMENT</b> A DISTRIBUTION UNLIMITED: PB Public Release					
<b>13. SUPPLEMENTARY NOTES</b>					
<b>14. ABSTRACT</b> This final report summarizes a three-year effort to develop and characterize quantum devices based on atomically thin two-dimensional semiconductor transition metal dichalcogenides. Devices consisting of hexagonal boron nitride encapsulated tungsten diselenide contacted by platinum were developed and characterized at low temperatures. Methods for successful process integration of six lithography steps, two 2D material transfers, and two annealing steps were developed. Annealing in forming gas was found to be crucial for both heterostructure quality and contact transparency. A technique for transfer of two-dimensional materials without subjecting them to high temperatures was also developed but it was found not to produce superior heterostructure quality compared with conventional techniques. Using a combination of a global accumulation gate and several local confining gates, quantum dots were routinely formed, which displayed quantized charging and, most importantly, quantized energy levels as revealed in transport measurements at mK temperatures. Analysis of typical charging energies and quantum level spacings indicates quantum dot diameters in the range of 20-50 nm, consistent with the lithographic dimensions of the device and the relatively large band gap of tungsten diselenide. We further observed that these devices could be populated with both electrons and holes, which offers opportunities for novel optoelectronic quantum devices.					
<b>15. SUBJECT TERMS</b>					
<b>16. SECURITY CLASSIFICATION OF:</b>			<b>17. LIMITATION OF ABSTRACT</b>	<b>18. NUMBER OF</b>	<b>19a. NAME OF RESPONSIBLE PERSON</b> POMRENKE, GERNOT
<b>a. REPORT</b>	<b>b. ABSTRACT</b>	<b>c. THIS PAGE</b>			

Standard Form 298 (Rev. 8/98)  
Prescribed by ANSI Std. Z39.18

DISTRIBUTION A: Distribution approved for public release.

Unclassified	Unclassified	Unclassified	UU	<b>PAGES</b>	<b>19b. TELEPHONE NUMBER</b> <i>(Include area code)</i> 703-696-8426
--------------	--------------	--------------	----	--------------	---

QUANTUM DEVICE LABORATORY

University of Arkansas

Fayetteville, AR 72701

*Final Technical Report*

Grant FA9550-16-1-0203

June 15, 2016 to June 14, 2019

**QUANTUM DEVICES BASED ON  
TRANSITION METAL DICHALCOGENIDES**

**PRINCIPAL INVESTIGATOR:**

**Dr. Hugh Churchill**

churchill@uark.edu (479) 575-7235

*Submitted to:*

**Dr. Gernot S. Pomrenke**

AFOSR/RTB1

Optoelectronics and Photonics

875 North Randolph Street

Arlington, VA 22203

## I. Introduction and Objectives

This is the final technical report of the AFOSR YIP project being carried out at the University of Arkansas Quantum Device Laboratory to investigate quantum devices such as quantum dots using 2D semiconductor transition metal dichalcogenides (TMDs) as the host material, covering the period from June 15, 2016 to June 14, 2019. The effort was divided into three primary objectives:

1. Fabrication of TMD quantum devices (gates, insulator, contacts, active layer)
2. Electronic transport characterization of TMD quantum devices (Coulomb blockade spectroscopy of spin-valley quantum levels)
3. Advanced optoelectronic manipulation of TMD quantum devices (layer blockade, single photon emission, characterization of potential spin-valley qubits)

Through heroic process development and integration efforts by the research team to overcome unanticipated challenges, we successfully accomplished the first two objectives stated above over the course of the funding period. These challenges, our solutions to them, accomplishments related to transport measurements, and the final status of the effort are described below. The most significant outcome of the research is the observation that our devices are capable of *ambipolar operation*, which has significant consequences for the future quantum optoelectronic applications of the device platform we have developed.

## II. Research Accomplishments

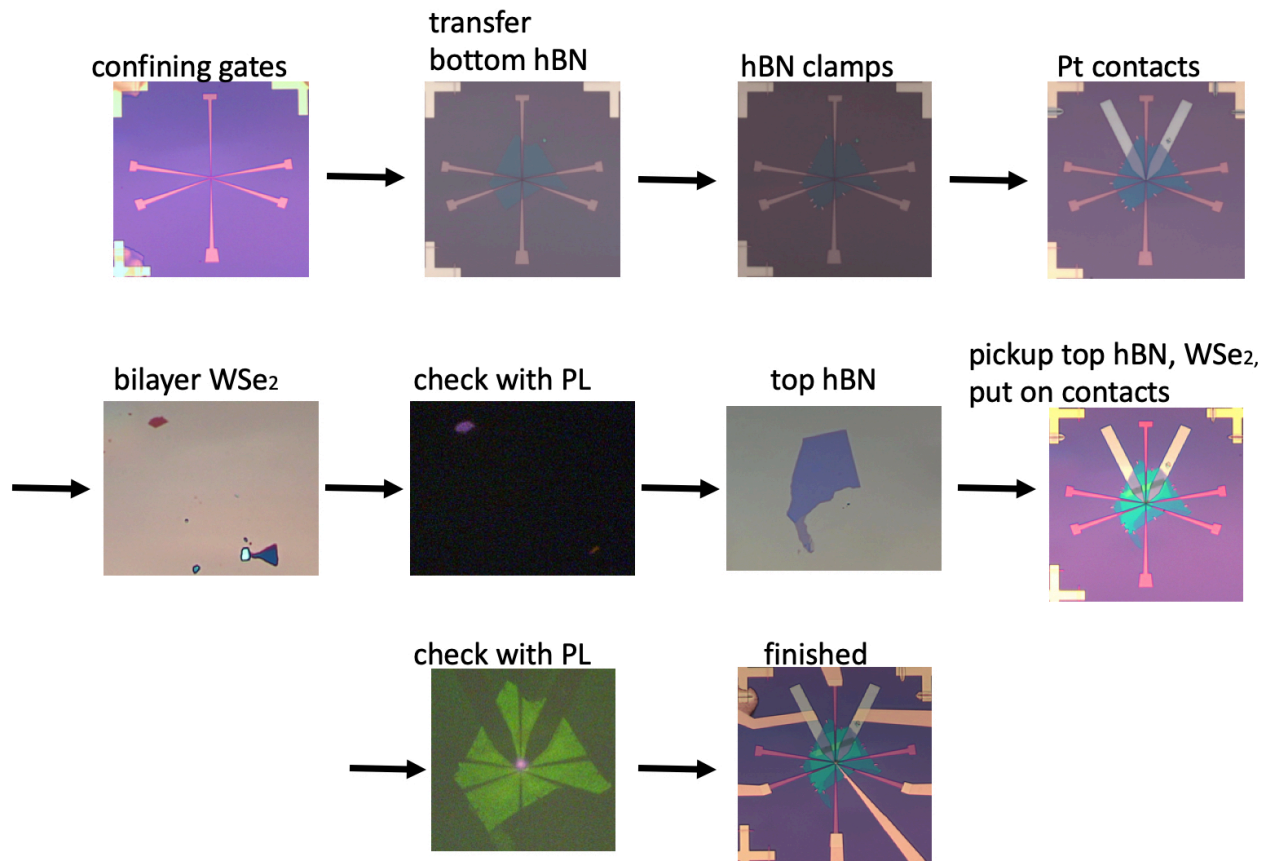
### *II.1 Successful quantum dot fabrication processes*

A majority of the effort in this project was devoted to developing the fabrication processes required to create TMD quantum devices. A summary of the final steps in the fabrication process is:

1. Patterning and metallization of alignment marks for electron beam lithography
2. Patterning and metallization of small (< 100 nm) quantum dot confinement gates
3. Transfer of thin (~10 nm) hBN gate insulator
4. Patterning and metallization of hBN clamps to prevent slippage during second transfer
5. Patterning and metallization of Cr/Pt TMD contacts
6. Annealing in forming gas to clean hBN and contact surface
7. Transfer of monolayer or bilayer WSe<sub>2</sub> (TMD) and protective top hBN insulator
8. Patterning and metallization of top accumulation gate
9. Patterning and metallization of bond pads
10. Second forming gas anneal to improve contact quality

These steps are illustrated with the images presented in Figure 1 below.

**Figure 1: Summary of final fabrication procedure for WSe<sub>2</sub> quantum dots.** All steps of the process are represented here except for the two annealing steps.



Our initially proposed plans for device fabrication required substantial modification, particularly with respect to contact fabrication, primarily because of the lack of a suitable and local reactive ion etching tool. The evolution of the process is summarized in Fig. 2 below. The primary finding in Year 3 with respect to contact fabrication was that Pt is far superior to Au as a bottom contact for WSe<sub>2</sub>. Once the Pt process was successfully developed, it contacted WSe<sub>2</sub> with 100% yield over 10 devices. The platinum process itself required substantial effort, given the high melting point of Pt and the lack of an ebeam evaporator at UA with a water-cooled substrate holder. By moving to ultrathin, 8 nm Pt, we were able to achieve clean liftoff and very flat Pt for successful WSe<sub>2</sub> contact.

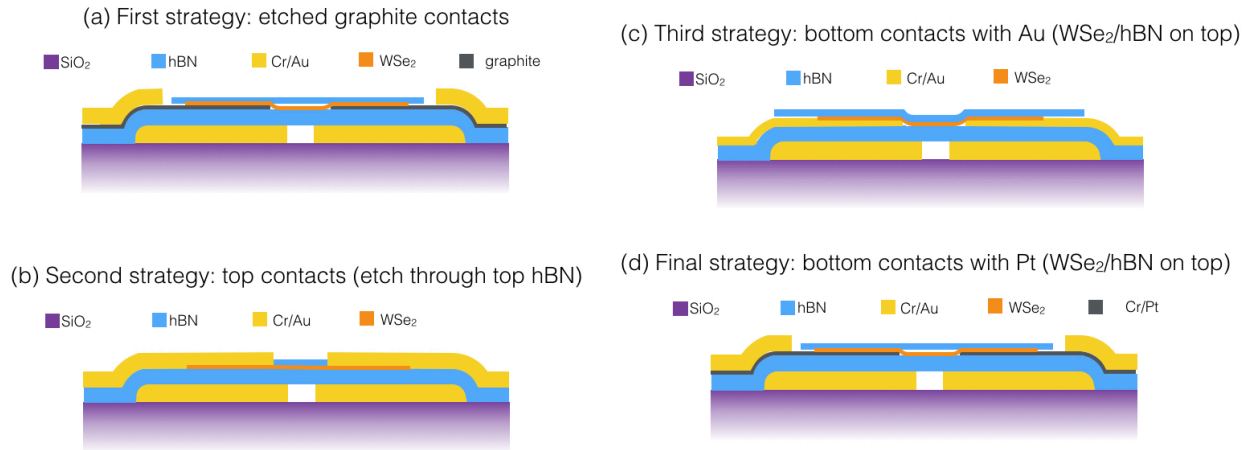


**Figure 2: Contacting strategies for WSe<sub>2</sub> quantum dots.** (a) The original strategy, in which graphite and hBN are laminated over quantum dot gates, then the graphite is etched over the dot area, and WSe<sub>2</sub> and hBN are placed over the graphite contacts. (b) A second strategy in which hBN/WSe<sub>2</sub>/hBN is placed over the gates, the top hBN is etched, and gold is deposited to contact the WSe<sub>2</sub>. (c) In a third strategy, gold contacts are pre-defined on the bottom hBN, then WSe<sub>2</sub>/hBN is placed over the contact metal. The advantage of this strategy is that no etch step is required, simplifying fabrication dramatically. (d) In the current and finally successful strategy, the gold bottom contacts are replaced with platinum, which has excellent performance at low temperature.

In our opinion the most important competitive advantage of the devices we fabricate relative to what has been reported in the literature is our insistence on placing contact metal very close to the quantum dot. This proximity eliminates the possibility of “accidental” quantum dots outside the gated region that inevitably form because of the disorder potential experienced by electrons propagating through an imperfect semiconductor. By placing the contact metal as close as possible to the dot, there is not sufficient lateral space for an accidental dot to form. These accidental dots generate spectroscopic features masking those of interest in the gated region of

the device; therefore, we are working quite hard to prevent them in our devices. Transport measurements presented later in this report demonstrates the success of this strategy.

Our initial device fabrication procedure required six lithography steps, two separate 2D heterostructure transfers, and an etch. At the end of Year 1, we were confident that process integration of these many steps would not pose a significant challenge; instead, we learned that it was difficult to produce a clean etched-graphite surface onto which to transfer the WSe<sub>2</sub> layer. In July 2017 we neared completion of a device following that procedure, but the hBN/graphite interface was not smooth, and the annealing procedure we used to smooth it out created tears in the graphite and destroyed the device.

After one more device fabricated in this way suffered similar problems, we then transitioned to a strategy in which the entire hBN/WSe<sub>2</sub>/hBN stack was transferred in one step, followed by an etch through the top hBN to deposit contact metal onto the exposed WSe<sub>2</sub>. The difficult aspect of this strategy is to etch through the top hBN but stop at the WSe<sub>2</sub> layer, which is only three atoms thick. Reactive ion etching with O<sub>2</sub> plasma selectively etches hBN over WSe<sub>2</sub> by about a factor of five, so the technique is possible, if challenging. We initiated etch tests locally at the UA HiDEC facility, but after about a month of development, the UA RIE tool became inoperable, with an indefinite repair timeline. We then chose to use the nanofabrication facility at the University of Pennsylvania remotely to measure etch rates of hBN, WSe<sub>2</sub>, PMMA, and ZEP (ebeam resist), using both pure O<sub>2</sub> plasma and O<sub>2</sub>/CHF<sub>3</sub> etch chemistries. Remote processing is slow, but we eventually collected enough etch rate data to see that while a viable process window existed for etching the top hBN without destroying monolayer WSe<sub>2</sub>, it was a

very small window, and likely many batches of devices would need to be fabricated for a successful outcome.

Therefore, in March 2018, we adopted our current strategy of simplifying the fabrication procedure by writing contacts prior to WSe<sub>2</sub> transfer [Fig. 2(c)]. This change reduced the number of required lithography steps from 6 to 4, and eliminated the need for an etch step, which is problematic to execute efficiently at UA. This change, combined with the addition of a second

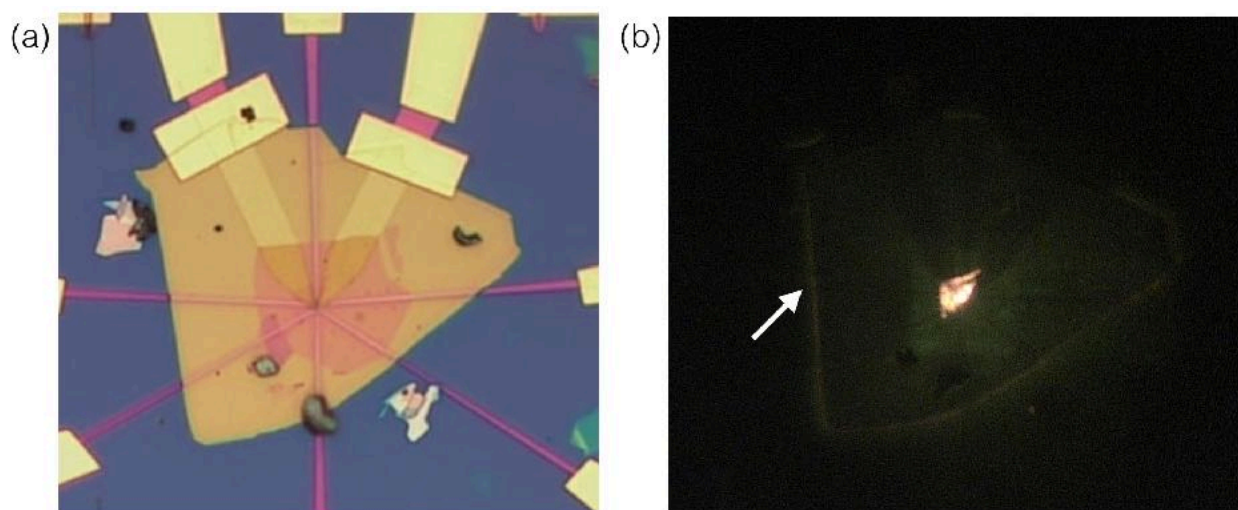


**Figure 3: Complete bottom-contact WSe<sub>2</sub> quantum dot device.** (a) Brightfield optical image of the first complete device. (b) PL image highlighting the monolayer WSe<sub>2</sub> flake well aligned with the contacts and confinement gates. Emitted light guided to the edges of the bottom hBN is highlighted with a white arrow.

graduate student to the fabrication team, has now enabled us to create complete devices in a reasonable period of time (Fig. 3). Globally, these devices are not as flat as those employing graphite contacts or by etching through hBN/WSe<sub>2</sub>/hBN stacks, but in the quantum dot region in the center of the device where flatness matters, the current generation of devices are just as good as those using other techniques, and they can be fabricated in a fraction of the time. Figure 3(a) shows an optical image of the completed device consisting of, from bottom to top: gates, bottom

hBN, contacts, WSe<sub>2</sub>, and top hBN. Figure 3(b) is a PL image of the same device highlighting the strong emission from the WSe<sub>2</sub> monolayer at the center of the device. Interestingly, the 70 nm-thick bottom hBN is fairly efficient at guiding some emitted light via total internal reflection to the edges of the hBN. This effect, if optimized, could be useful for future integrated photonics applications of TMD quantum devices.

One important piece of information we learned through initial, room temperature transport measurements with this first device is that the quantum dot confining gates are not sufficiently strong by themselves to induce appreciable hole density in the quantum dot. Instead, an additional gate placed over the top hBN is required to induce holes in the WSe<sub>2</sub>, which can then be depleted using the confining gates. For simplicity, this gate will be made with thick gold for transport-based WSe<sub>2</sub> quantum dots, but for future devices targeting optoelectronic measurements, the top gate will be made transparent using graphene. Alternatively, we can invert the fabrication stack and place the accumulation gate on the bottom with the confining gates on top, which will also permit optical access.

## *II.2 Low-temperature 2D material transfer*

To prevent fragile 2D materials from cracking during heterostructure assembly, we have developed a microscopic laser cutting technique to complete the final heterostructure transfer onto the target substrate. In the practice commonly used by most 2D material research groups, flakes of individual 2D materials are picked up and stacked with a thermoplastic such as polycarbonate supported by a silicone stamp. To transfer the heterostructure onto some target substrate (such as the confining gates in our effort), the thermoplastic is heated about its melting

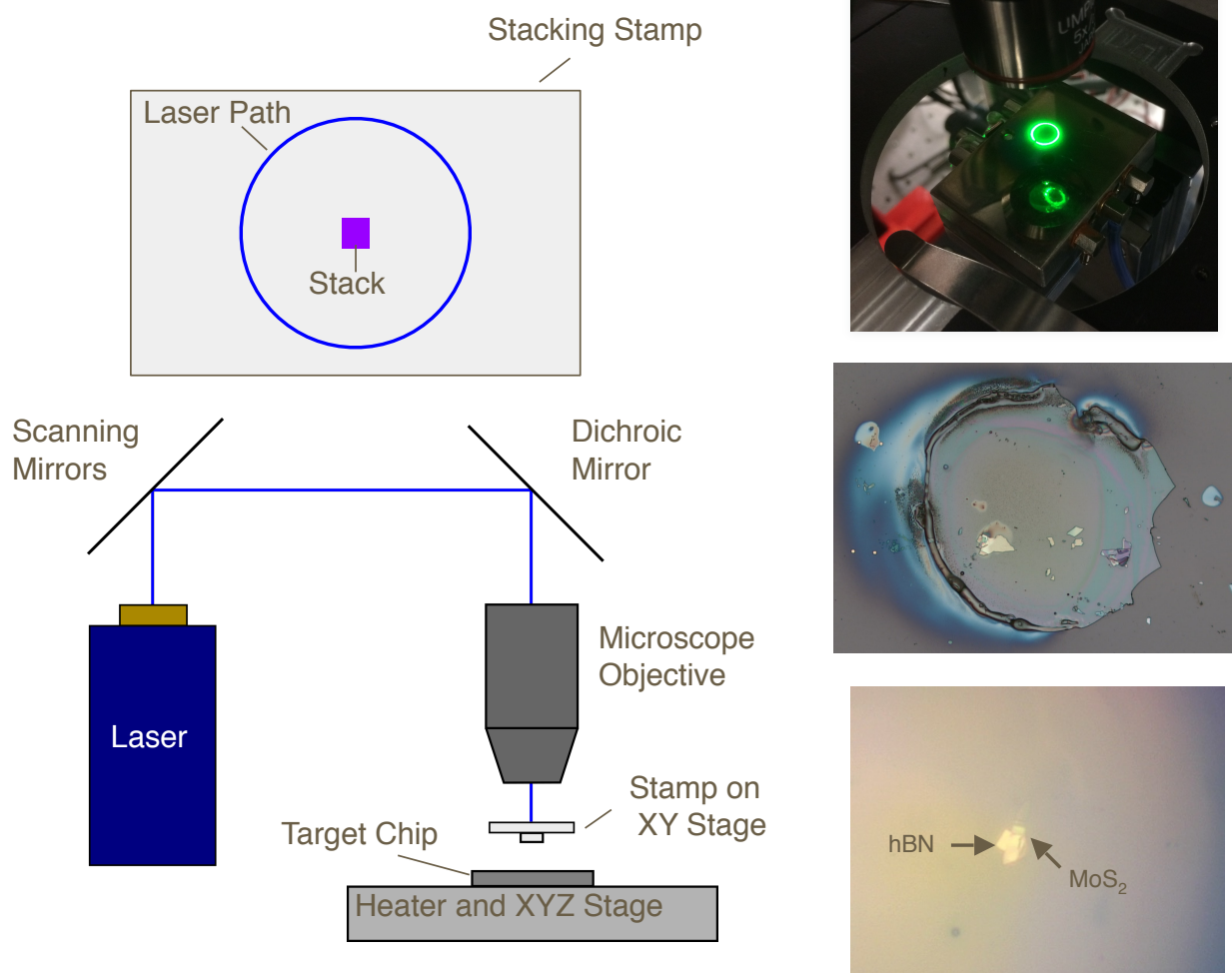


**Figure 4:** Left, schematic of microscopic laser cutting apparatus for thermally protected transfers of 2D material heterostructures onto target substrates. Top right, focused circular beam projected onto the sample. Middle right, polycarbonate film cut out from transfer stamp by melting a perimeter around the heterostructure. Bottom right, completed transfer of hBN/MoS<sub>2</sub> heterostructure onto a silicon target chip.

point (150° C) so that it releases from the silicone, trapping the 2D heterostructure on the target substrate. Because of the very large thermal expansion coefficients of thermoplastics, this heating process applies significant strain to the 2D heterostructure and often fractures non-graphene 2D materials. These fractures significantly reduce device yield. For simple devices

such as Hall bars and three-terminal FETs, such as losses are acceptable, but for more complicated devices with many fabrication steps such as quantum dots, this loss mechanism must be avoided.

Our approach is summarized in Fig. 3. A violet diode laser (405 nm) is scanned in a circular pattern using high-speed galvo mirrors driven by a homemade function generator (openDACs.com) with controllable XY position and amplitude. A dichroic mirror directs the laser beam into a microscope objective, which projects a 10  $\mu\text{m}$  to 1 mm diameter annulus with a diffraction-limited perimeter width onto the sample. The intense beam melts the thermoplastic (polycarbonate) around the perimeter of the heterostructure. When the silicone transfer stamp is withdrawn from the target, the melted perimeter pins the thermoplastic to the target, completing the transfer. In many heterostructure transfers using this technique, we have not yet observed evidence of cracking, but further testing of the technique revealed that it is not superior to traditional stacking methods, and we have abandoned the technique.

### *II.3 Dilution refrigerator filtering*

A major emphasis of the effort was dedicated to completing laboratory infrastructure requirements for the planned measurements. During Year 2, wiring and filtering of the dilution refrigerator was completed by one of the graduate students supported by this award, Jeb Stacy. High quality filtering is required to obtain low electron temperatures, given the difficulty at mK temperatures of achieving good thermalization between the electrons in the device and the coldest part of the dilution refrigerator, the mixing chamber. The filtering strategy we have

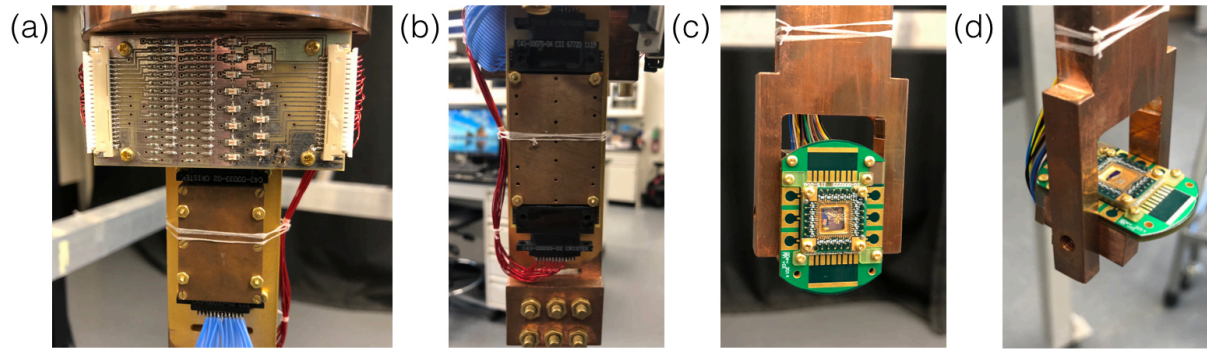


**Figure 5: Dilution refrigerator filtering.** (a) two-stage RC (top) and copper-powder (bottom) filters. (b) seven-stage  $\pi$  filters. (c) Coldfinger in parallel field configuration. (d) Coldfinger in perpendicular field configuration.

employed, shown in Fig. 5, uses a state-of-the-art, three-component configuration, with each component targeting a different frequency range for noise suppression. The first component of the filtering strategy consists of two-stage RC filters targeting audio frequencies, followed by a second component consisting of seven-stage  $\pi$  filters that suppress radio frequencies, and finally a third-stage copper powder filter that attenuates microwave frequencies, up to approximately 20 GHz. The success of this filtering strategy will be evaluated using Coulomb blockade thermometry when the first quantum dot devices are measured at low temperature. Jeb also installed a rotate-able copper coldfinger on the dilution refrigerator that allows measurements in any magnetic field direction between perpendicular field (for Hall measurements) and parallel field (for Zeeman spectroscopy), as shown in Fig. 5 (c) and (d).

To complete the dilution refrigerator setup, in April 2018 we received a Cryomech PT415 helium reliquefier purchased with equipment funds from this award. This reliquefier will dramatically reduce liquid helium costs (up to 95%) associated with running the dilution

refrigerator by recondensing boil-off gas back into the dewar. The installed system beats specifications and is able to reliquefy 18 L/day of room temperature gas and 32 L/day of cold boil-off gas.

#### *II.4 Optical cryostat installation*

In December 2017 we received the optoelectronic cryostat (Fig. 2) in which we will perform the optoelectronic measurements planned for this end of this project. This cryostat has a base temperature of 2 K and applies magnetic fields up to 8 T, while permitting high-NA imaging and spectroscopy on WSe<sub>2</sub> quantum devices.

Graduate assistant Jeb Stacy spent the first half of Year 2 working on completion of cryostat setup and wiring. With those activities complete, he joined the other graduate student, Shiva Davari, on fabrication tasks to accelerate that effort, as described below.

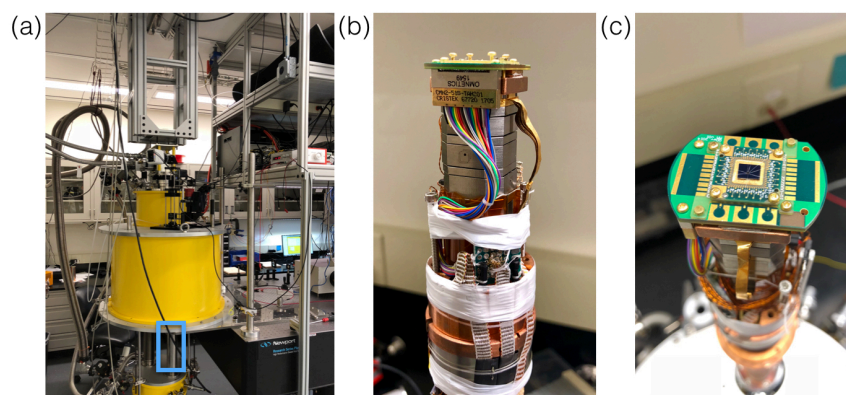


**Figure 6: Optical cryostat.** (a) Image of the cryostat, with ceiling-mounted coldhead to minimize vibrations. The sample area (blue square) is inserted into the room-temperature bore of the magnet. (b) 3-axis nanopositioner plus xy-scanner for imaging. (c) Top view of the sample PCB, which is cross-compatible with the dilution refrigerator PCB shown in Fig. 5.

## II.5 Gate Lithography

Observing resolved quantum levels of a WSe<sub>2</sub> quantum dot crucially depends on small dot size because of the relatively large mass of WSe<sub>2</sub> holes (compared to GaAs electrons, for example) and the inverse relationship between dot size and quantum level spacing. Our ability to create small quantum dots has been significantly improved in the past year with the installation of a JEOL JBX-5500 50 kV electron beam lithography system (shown in Fig. 3) into the same building as the Quantum Device Lab in early 2017. This system was moved from another location on campus, and because of problems with the re-installation, we were not able to fully take advantage of this instrument until the beginning of the current performance period. Since that time, the two graduate students and one undergraduate student working on this project have become experts in electron beam lithography, and in fact have become the primary source of

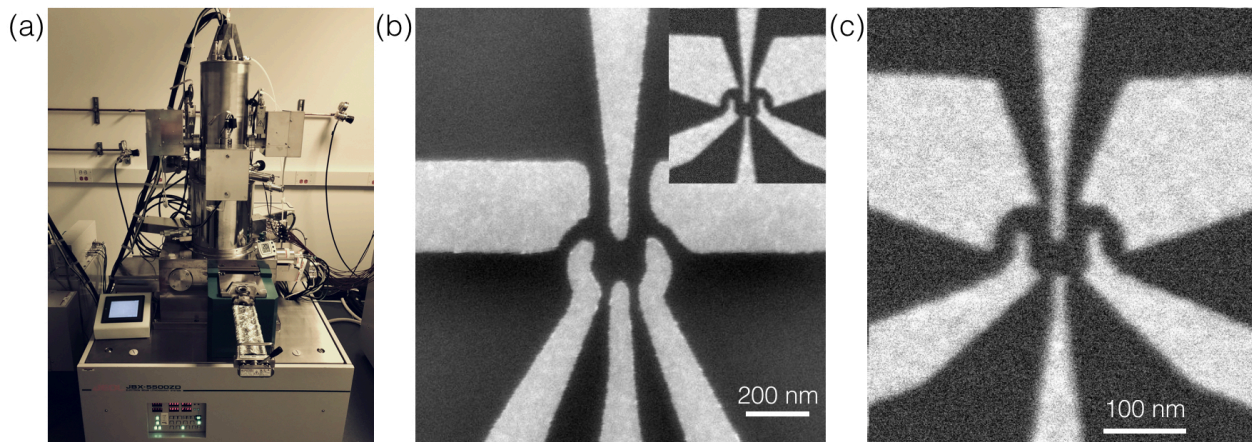


**Figure 6: Electron beam lithography.** (a) JEOL JBX-5500 electron beam lithography system housed in the UA Nano Institute. (b) Quantum dot gate design reported in the Year 1 report. Inset: current design on same scale. (c) Current gate design, smaller than the earlier one by more than a factor of two.

expertise to train and consult the UA EBL user group across campus, which now numbers more than fifteen users. This high-resolution machine, combined with high-resolution EBL resists ZEP and CSAR, have allowed us to reduce the lateral dimensions of our quantum dot gate design by more than factor of two without sacrificing yield [Fig. 3(b) and (c)].

### *II.6 Exfoliation of Large-area WSe<sub>2</sub>*

Heterostructure assembly, described below, becomes much easier when the lateral size of mechanically exfoliated flakes can be made the larger than the few-micron minimum required for accurate placement in a diffraction-limited optical microscope. We have successfully adopted a procedure first reported by Ali Javey and coworkers for gold-mediated exfoliation of large-area TMD monolayers to produce large WSe<sub>2</sub> with bright PL, as shown in Fig. 7. This procedure significantly reduces “flake hunting” effort and facilitates incorporation of WSe<sub>2</sub> into van der Waals heterostructures. Unfortunately, for quantum device applications, we have observed that the crystal quality of flakes obtained by this method is not as good as that achieved with standard exfoliation.

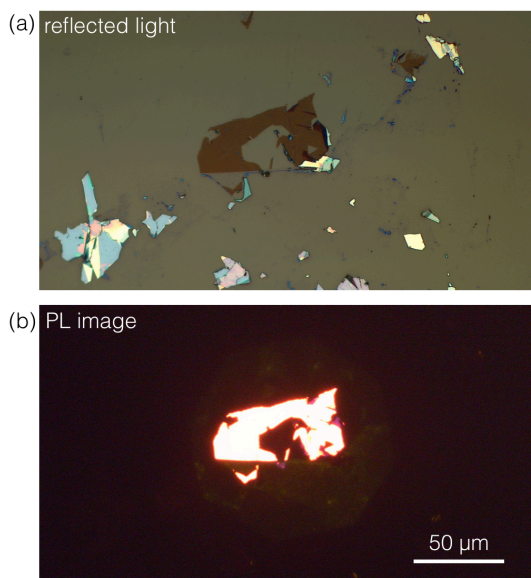


**Figure 7: Large-area WSe<sub>2</sub> exfoliation.** (a) Using gold-mediated exfoliation in which gold is evaporated on thick WSe<sub>2</sub>, peeled off, and etched away, large-area flakes of WSe<sub>2</sub> are left behind because of a strong affinity of the top layer of WSe<sub>2</sub> for evaporated gold. (b) Photoluminescence of the WSe<sub>2</sub> flake; high brightness confirms a direct-gap monolayer.

## II.7 UV-ozone cleaning of transferred hBN

To maintain high mobility and a mean free path larger than the width of the dot, our devices require an atomically flat hBN substrate onto to which we transfer monolayer WSe<sub>2</sub>. Occasionally, the polycarbonate transfer polymer used to place the hBN over the quantum dot confining gates is not completely removed after solvent cleaning [Fig. 8(a)]. In this situation, we have discovered that UV-ozone cleaning is very effective at removing polycarbonate residue without roughening the hBN surface [Fig. 8(b)], as would more aggressive treatments such as O<sub>2</sub> plasma etching. This technique significantly improves yield and throughput of our fabrication efforts.

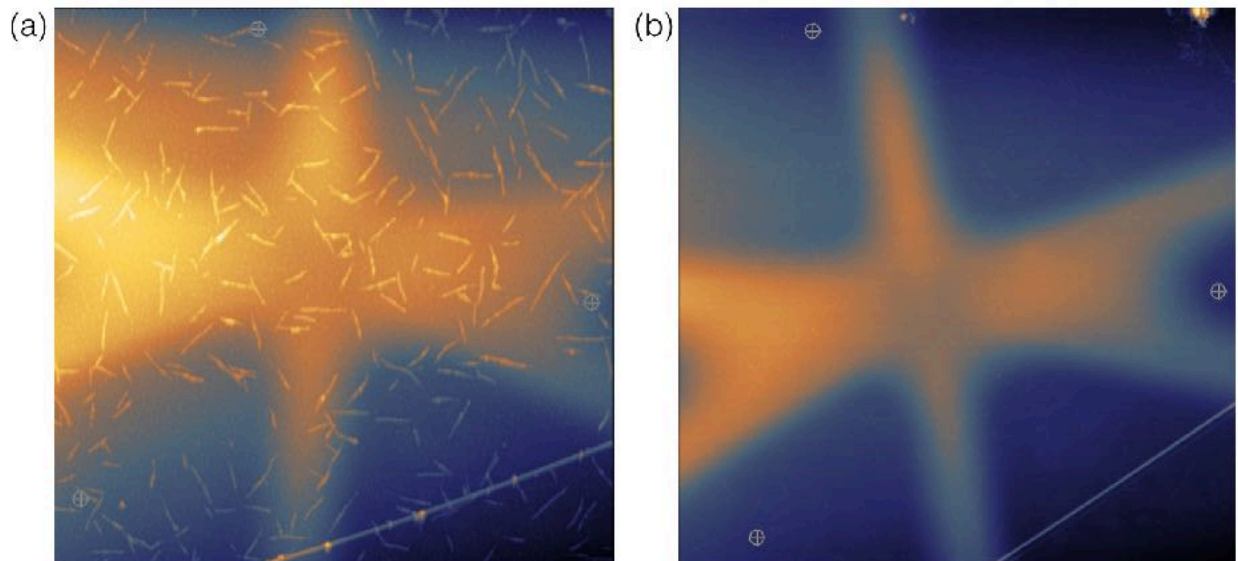


**Figure 8: UV-ozone cleaning of transferred hBN.** (a) AFM image of as-transferred bottom hBN over quantum dot confining gates, following overnight chloroform soak to dissolve polycarbonate transfer polymer, followed by cleaning in acetone and IPA. (b) AFM image of the same hBN flake after treatment in UV-ozone, followed by an acetone and IPA clean. Remaining topography evident in the image is caused by draping of the hBN over the quantum dot gates. In the center region where the dot is defined, the hBN height varies smoothly by only a few nm because of the relatively thick hBN used.

## II.8 Transport characterization of monolayer and bilayer WSe<sub>2</sub> quantum devices

Putting all the fabrication pieces together, in the final year of the project, we have measured four monolayer or bilayer devices at low temperature. Two significant results have come out of these measurements. First, we have observed Coulomb blockade with both electrons and holes in the same device by adjusting the voltage on the accumulation gate, which opens up significant potential for the creation of future quantum optoelectronic devices based on designs similar to the ones we have demonstrated in this project. Second, we have observed discrete quantum levels in the quantum dot, which has not been accomplished previously, and which is a prerequisite for application of this material for qubit development.

Ambipolar conduction is demonstrated in Fig. 9 below. As the voltage applied to the

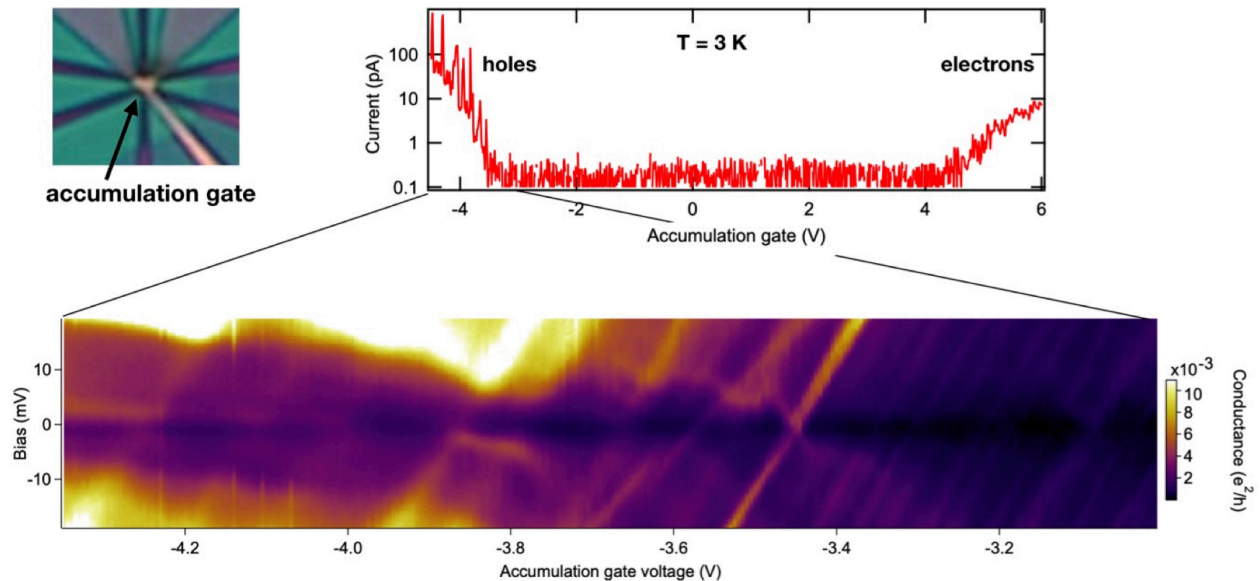


**Figure 9: Demonstration of ambipolar quantum transport in a WSe<sub>2</sub> quantum dot.** Upper left panel: optical image of a representative device illustrating the location of the accumulation gate that tunes the carrier density in the quantum dot. Upper right panel: current (log scale) as a function of accumulation gate voltage. Lower panel: differential conductance  $dI/dV$  as a function of source-drain bias and accumulation gate voltage demonstrating Coulomb blockade.

accumulation gate is adjusted from large negative voltages to large positive voltages, the quantum dot switches from holding holes, to being neutral, and finally to holding electrons. In the range of gate voltages between -3.6 and -3.0 V, well-resolved Coulomb blockade peaks with additional, higher-energy resonances indicating quantum energy levels are observed, and for more negative gate voltages, the behavior transitions to a more open regime, likely of a mixed-valence nature.

At lower temperatures, these states become much better resolved, and excited state conductance resonances are unambiguously identified. Figure 10 displays conductance through one sample at a temperature of 50 mK. The ground-state/excited-state pair highlighted in the figure is split by 2.5 meV at zero magnetic field. This splitting corresponds to a quantum dot diameter of 20 nm assuming an effective mass for holes in WSe<sub>2</sub> of 0.4  $m_0$ , which is reasonable considering the lithographic dimensions of the dot and the strong confinement providing by the relatively large band gap of WSe<sub>2</sub>. The dot size can also be estimated from the charging energy, which is approximately 5 meV for the charge states shown in Fig. 10. Calculating the capacitance for 8 nm-thick hBN and using the charging energy formula  $E_C = e^2/C$ , we expect a diameter of 100 nm. Therefore, the level resolved in Fig. 10 may not be the first excited state, but instead corresponds a higher excited state of the dot. Future experiments will resolve this question.

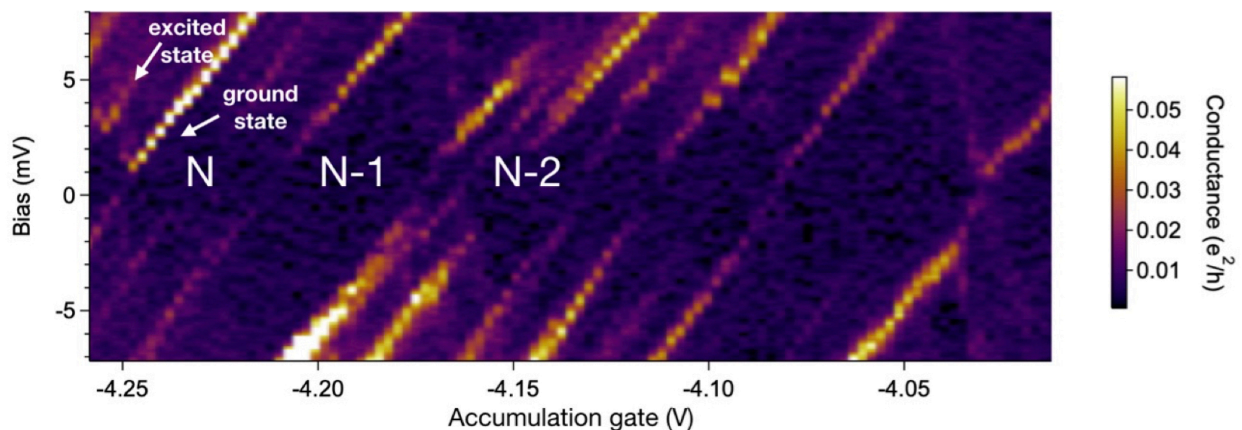


**Figure 10: Resolved quantum energy levels of a bilayer WSe<sub>2</sub> quantum dot.** Conductance as a function of source-drain bias and accumulation gate voltage at 50 mK shows well-resolved charge states for holes as well as excited state transport.

We display results from another device, this time a monolayer in Fig. 11. Transport characteristics of this device are largely similar to those of the bilayer shown in Fig. 10.

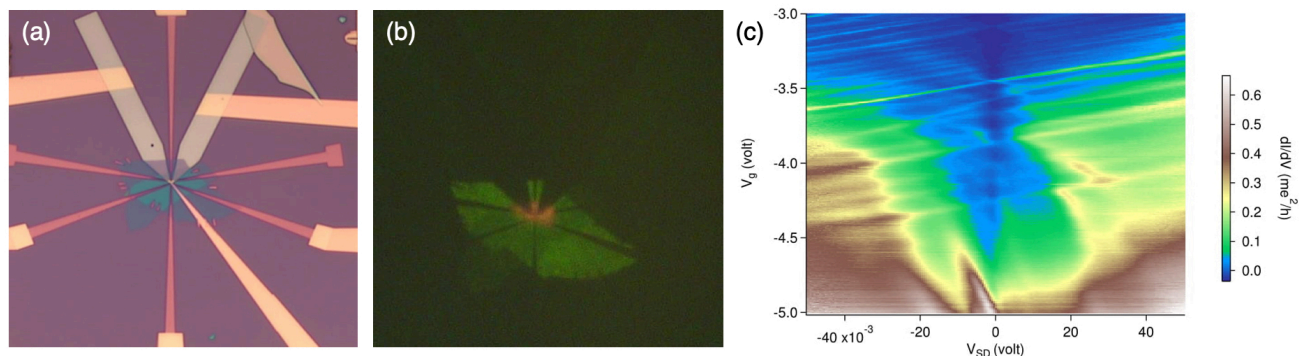


**Figure 11: Monolayer WSe<sub>2</sub> device and transport at 4 K.** (a) Completed monolayer WSe<sub>2</sub> device. (b) Photoluminescence image of the device in (a). (c) Conductance as a function of accumulation gate voltage and source-drain bias at 4 K.

### III. Summary of Effort

After meeting significant process integration challenges related to contacting monolayer WSe<sub>2</sub> in a complete quantum dot device, we ultimately succeeded in developing processes to create state-of-the-art TMD quantum devices. Ambipolar quantum transport was demonstrated, which will enable the creation of future quantum optoelectronic devices. Transport measurements at mK temperature revealed excited states of these quantum dots for the first time, an important milestone in the development of optoelectronic TMD quantum dots. A team of four people—graduate students Jeb Stacy and Shiva Davari, joined by undergraduates Alejandro Mercado and Jeremy Tull—are all trained in every aspect of device fabrication and now efficiently able to write tiny gate patterns, transfer 2D material heterostructures, identify and characterize WSe<sub>2</sub> monolayers and bilayers, and contact those materials using electron beam lithography with better than 50 nm overlay accuracy. We look forward to leveraging this

expertise in the near future to explore quantum optoelectronic devices based on a variation of the designs established in this project.

#### **IV. Personnel Supported** (all in Department of Physics, University of Arkansas)

**Faculty:** Hugh Churchill

**Graduate Students:** Shiva Davari and Jeb Stacy

**Undergraduate Students:** Hamilton Johnson, Alejandro Mercado, Jeremy Tull

#### **V. Publication and Patent**

##### **Publication:**

H. O. H. Churchill, G. J. Salamo, S.-Q. Yu, T. Hironaka, X. Hu, J. Stacy, and I. Shih, “Toward Single Atom Chains with Exfoliated Tellurium,” *Nanoscale Research Letters* **12**, 488 (2017).

##### **Patent:**

Our provisional application, “Growth and Characterization of Single Atom Chains for Future Nano-Electronics and Quantum Circuits,” was submitted as a full application (Serial Number 62/466074) on March 2, 2018.

##### **Presentations:**

This work has been presented at condensed matter seminars at Missouri State University, University of Tulsa, University of Maryland, University of Oklahoma, Texas A&M University, University of Texas, and New York University.

#### **VI. Honors**

University of Arkansas Honors College Research Grant, three awards, 2016-2018 (Alejandro Mercado)

University of Arkansas Graduation with Honors, *summa cum laude* (Alejandro Mercado)

Powe Junior Faculty Award, Oak Ridge Associated Universities, 2017 (Hugh Churchill)

University of Arkansas Chancellor's Innovation and Collaboration Fund, "Toward Efficient and Broadband Terahertz Sources with Ultrathin Black Phosphorus" (Hugh Churchill)

University of Arkansas Chancellor's Commercialization Fund, "Development of a silicon wafer platform for graphene energy harvesting (GEH) and measurement of its output power" (Hugh Churchill)

National Science Foundation CAREER Award (Hugh Churchill)

Presidential Early Career Award for Scientists and Engineers (Hugh Churchill)